3D-Var Assimilation Experiments with Flow-Dependent Dynamical Constraints

M. RESZKA✉, S. POLAVARAPU and Y. ROCHON (†Environment Canada, Toronto, Canada)

1 Introduction

1.1 Motivation

Repeated insertion of observations in any global data assimilation system is known to induce spurious mixing and to increase the speed of the stratospheric meridional overturning circulation, as compared with observations and model free simulations. This has an adverse effect on a number of standard diagnostics such as tracer distribution and the age of air, and poses a significant challenge in studies of long-term trends. In a recent comparison of the stratospheric circulation modelled by chemical transport models driven by analysed winds [1] improvements in the specification of the dynamical background-error constraints were cited as one of the chief ways in which these difficulties may be addressed. In particular, the Charney nonlinear balance and Quasigeostrophic (QG) omega equation can be used [2] to replace the static, regression-based constraint [3] traditionally used in atmospheric assimilation.

1.2 Flow-dependence

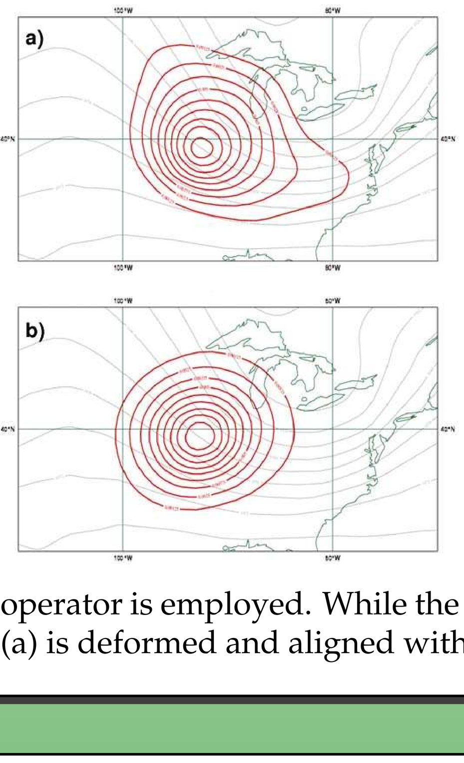

Flow-dependence of increments is a desireable feature from a physical standpoint, and can be illustrated through one-obs experiments as, for example, those at the European Centre for Medium-Range Weather Forecasting (ECMWF). The figure is adapted from [2]. Red contours show temperature increments corresponding to a single observation in geopotential height, while grey contours show the background geopotential height field as a proxy for the path of the jet stream, which is highly curved in this region. In panel (a) the Charney and QG omega balances are used, and in (b) the usual regression-based balance operator is employed. While the increment in (b) is roughly circular, the one in (a) is deformed and aligned with the background flow.

1.3 Tangent-linear constraints in η-coordinates

With some approximation, the balanced temperature and velocity potential increments δT_B, $\delta\chi_B$, resp., can be obtained from the streamfunction increment $\delta\Psi$ and background state (T_r, p, p_s, $\mathbf{u}_r = (u_r, v_r)$, $\zeta_r = \mathbf{k}\cdot\nabla\times\mathbf{u}_r$) using the following tangent-linear (TL) equations in the hybrid vertical coordinate η

- Charney and hydrostatic balance equations

$$\nabla_\eta^2\delta\Phi_B = \nabla_\eta\cdot(f\nabla_\eta\delta\Psi) - \nabla_\eta\cdot\left[RT_r\nabla_\eta\left(\frac{\delta p}{p}\right)\right] - \nabla_\eta\cdot\left[R\delta T\nabla_\eta\ln\left(\frac{p}{p_0}\right)\right]$$
$$+2(\widehat{\mathbf{z}}\times\nabla_\eta u_r)\cdot\nabla_\eta\left(\frac{1}{a\cos\phi}\frac{\partial\delta\Psi}{\partial\lambda}\right) + 2\nabla_\eta v_r\cdot\left[\widehat{\mathbf{z}}\times\nabla_\eta\left(-\frac{1}{a}\frac{\partial\delta\Psi}{\partial\phi}\right)\right] \quad (1)$$

$$\delta T_B = -\frac{p}{R}\frac{\partial\eta}{\partial p}\frac{\partial\delta\Phi_B}{\partial\eta} \quad (2)$$

- adiabatic QG omega and continuity equations

$$\nabla_\eta^2\delta\omega_B + \frac{f^2}{\sigma p_0^2}\frac{\partial^2\delta\omega}{\partial\eta^2} = \frac{f}{\sigma}\frac{\partial\eta}{\partial p}\frac{\partial}{\partial\eta}\left[\nabla_\eta\cdot(\mathbf{u}_r\delta\zeta) - B(\eta)\frac{\partial\eta}{\partial p}\frac{\partial\delta\zeta}{\partial\eta}\nabla_\eta\cdot(\mathbf{u}_r p_s)\right]$$
$$+\frac{f}{\sigma}\frac{\partial\eta}{\partial p}\frac{\partial}{\partial\eta}\left[\nabla_\eta\cdot(\delta\mathbf{u}(f+\zeta_r)) - B(\eta)\frac{\partial\eta}{\partial p}\frac{\partial\zeta_r}{\partial\eta}\nabla_\eta\cdot(\delta\mathbf{u}p_s)\right]$$
$$+\frac{R}{\sigma p}\nabla_\eta^2\left[\nabla_\eta\cdot(\mathbf{u}_r\delta T_B) - B(\eta)\frac{\partial\eta}{\partial p}\frac{\partial\delta T_B}{\partial\eta}\nabla_\eta\cdot(\mathbf{u}_r p_s)\right]$$
$$+\frac{R}{\sigma p}\nabla_\eta^2\left[\nabla_\eta\cdot(\delta\mathbf{u}T_r) - B(\eta)\frac{\partial\eta}{\partial p}\frac{\partial T_r}{\partial\eta}\nabla_\eta\cdot(\delta\mathbf{u}p_s)\right] \quad (3)$$

$$\nabla_\eta^2\chi_B = -\frac{\partial\eta}{\partial p}\frac{\partial\delta\omega_B}{\partial\eta} \quad (4)$$

where σ = static stability parameter, R = dry gas constant, p_0 is a constant reference pressure and $B(\eta)$ is specific to the hybrid coordinate. (1) with the condition $\delta\Phi_B(\eta = 0) \equiv 0$ also provides a balanced surface pressure increment. Neglecting the last two terms in (1) yields the Linear Balance.

In this study, experiments are performed with the 3D variational (3D-Var) data assimilation system of the Canadian Meteorological Centre (CMC) and the GEM-Strato forecast model, using the following TL balance constraints:

- SB - statistical, regression-based constraint (control)
- LB - Linear balance
- CB - Charney balance
- QG - QG omega balance

CBQG refers to experiments with both the CB and QG constraints.

2 One-obs experiments

2.1 Linear and Charney balance

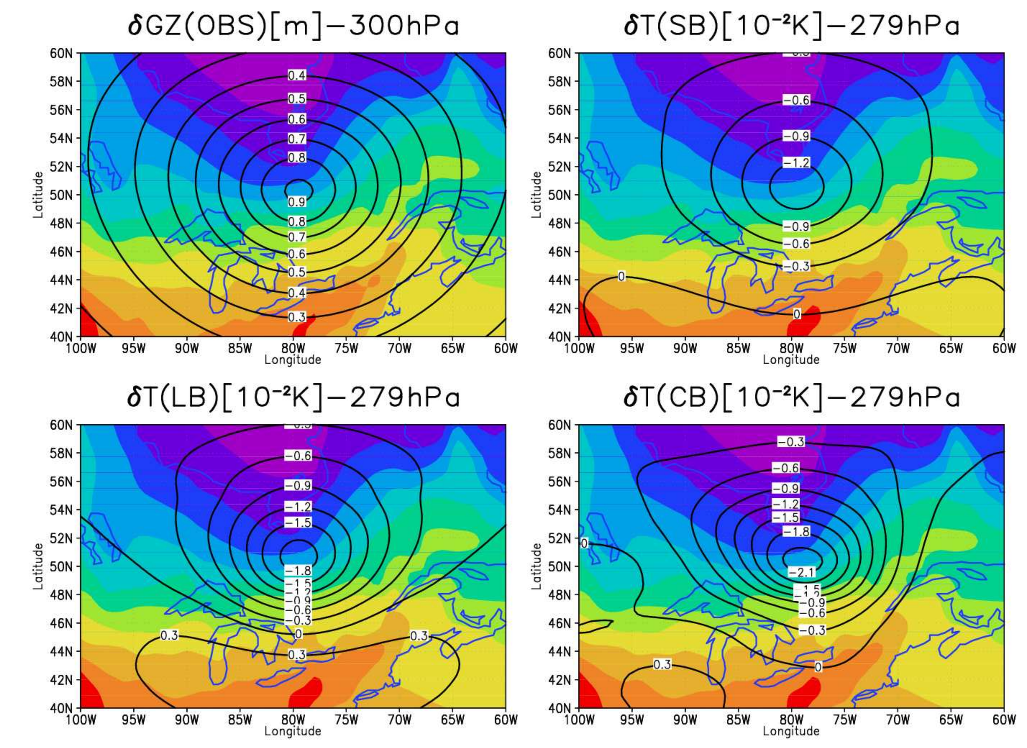

Black contours show horizontal sections of a single, specified observation in geopotential height δGZ(OBS) and the corresponding temperature increments δT obtained using the SB, LB and CB dynamical constraints. Color shading shows the background geopotential height (same in all plots) as a proxy for the mean flow. As expected, LB is similar to the control case SB, although its structure is more focused at the observation location. In the CB case the increment is deformed and, to some degree, aligned with the path of the background winds.

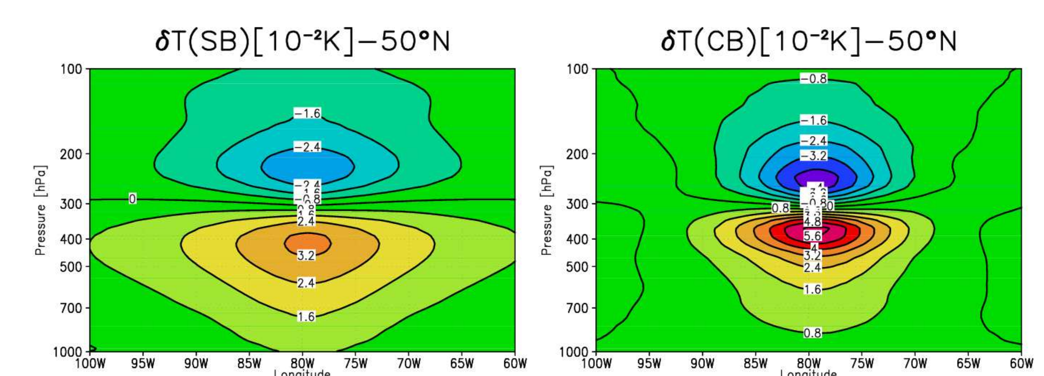

The vertical structure of δT in the SB and CB cases is shown. While qualitatively similar, the increment in case CB is more intense and compact than in case SB, both horizontally and vertically. Case LB (not shown) is intermediate between SB and CB.

2.2 QG omega balance

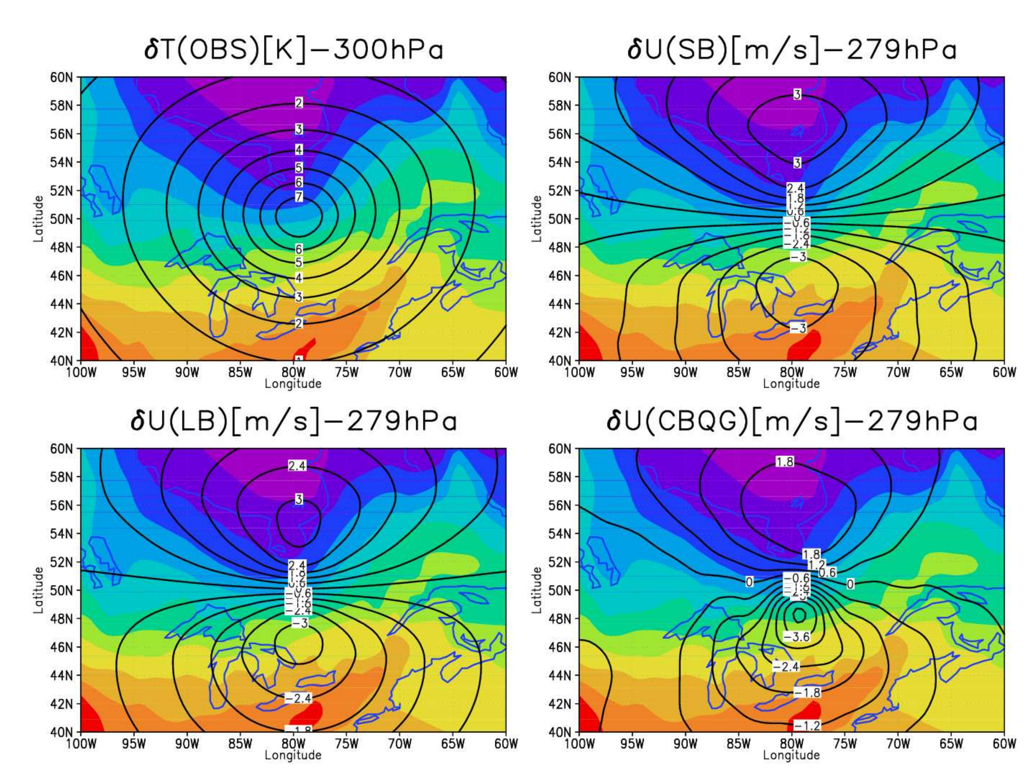

Black contours show horizontal sections of a single, specified observation in the temperature, δT(OBS), and the corresponding zonal velocity increments δU obtained using the SB, LB and CBQG constraints. Color shading shows the background geopotential height (as in section 2.1). As above, LB is similar to the control case SB and does not exhibit any asymmetry due to the background flow. In the CBQG case the increment shape and alignment are both influenced by the mean winds. The QG omega constraint additionally induces some small scale structure on the increment due to local divergent motions.

3 Time-mean correlations

3.1 Equinox conditions

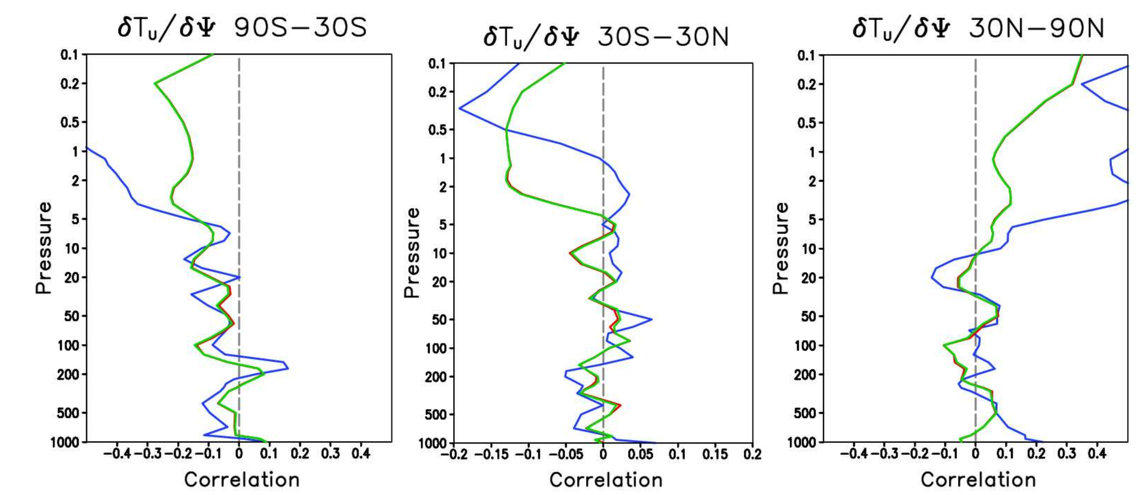

Monthly-averaged correlation of the unbalanced temperature δT_U with the streamfunction $\delta\Psi$ under September conditions obtained from an assimilation cycle which uses the SB (blue curves), CB (red curves) and CBQG (green curves) constraint. Correlations were averaged spatially over 3 distinct latitude bands: 90S–30S, 30S–30N and 30N–90N. For an accurate balance, the correlation should be small, i.e. the change of variable employed in the 3D-Var scheme should decorrelate the control variables (see e.g. [3]). Constraint CB consistently yields smaller correlations than SB in a number of regions, particularly in the upper stratosphere/lower mesosphere. The QG constraint does not make a significant contribution in this case.

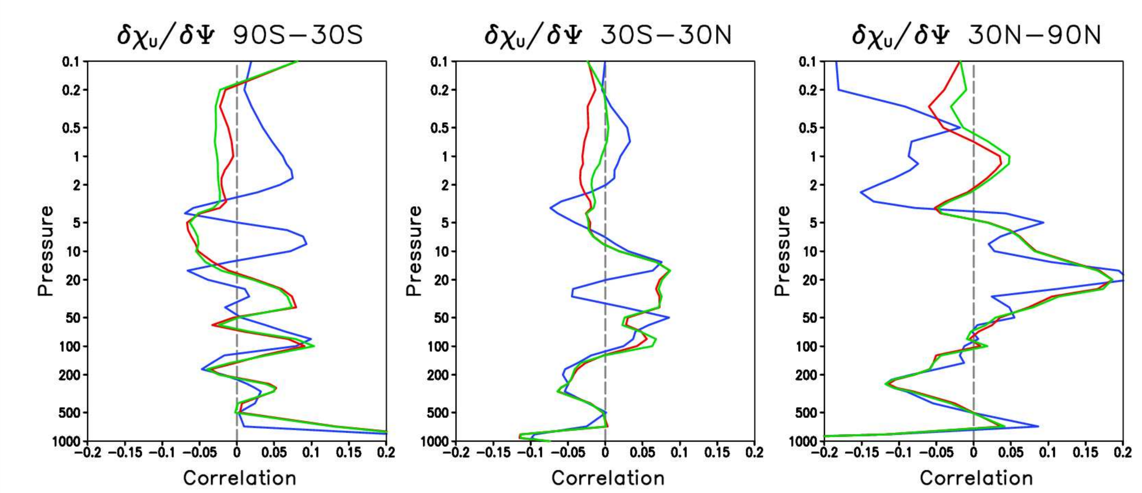

Correlations between $\delta\chi_U$ and $\delta\Psi$ are also generally smaller with CB than with SB at higher altitudes. The additional QG constraint has a small but significant impact above approx. 5 hPa, positive in tropics, negative in the southern hemisphere, and mixed in the northern hemisphere.

3.2 Solstice conditions

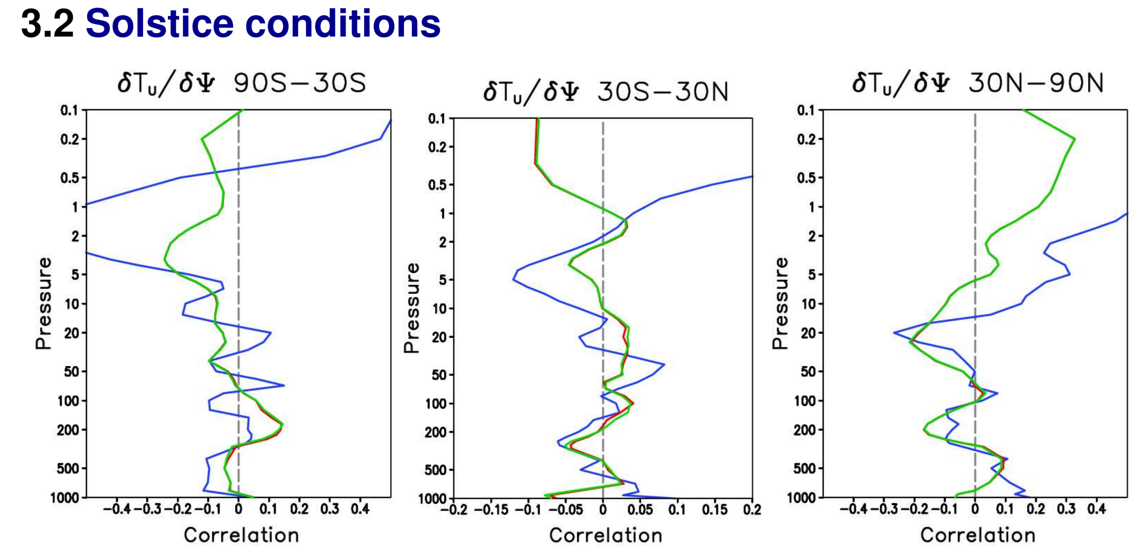

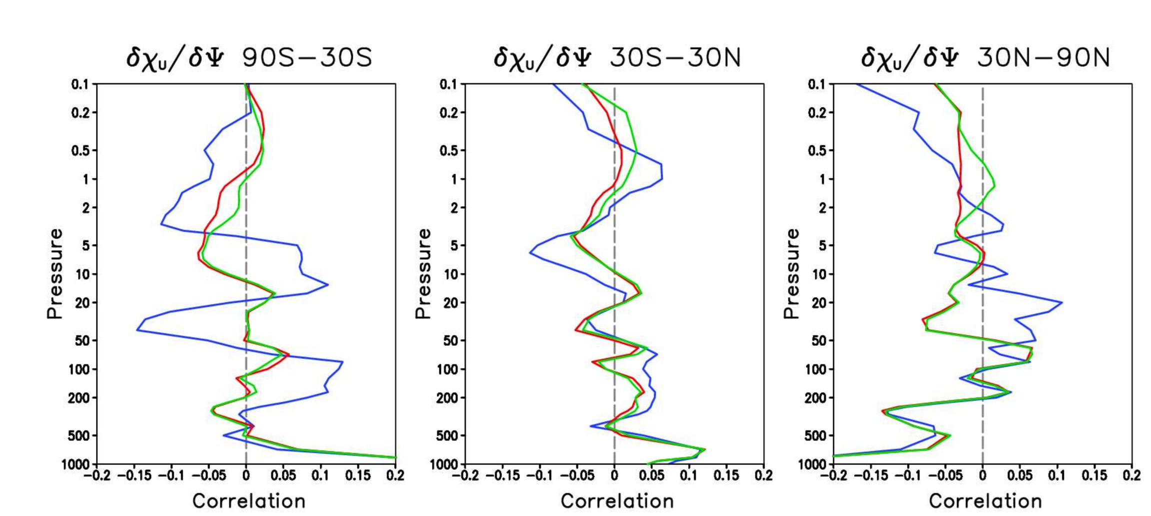

Correlations of δT_U with $\delta\Psi$ and $\delta\chi_U$ with $\delta\Psi$, as in section 3.1, but under January conditions. Correlations tend to be smaller in the CB and CBQG cases than the control in the southern hemisphere and the tropics. In the northern hemisphere an improvement is only evident in the mesosphere.

4 Time-mean scores against radiosondes

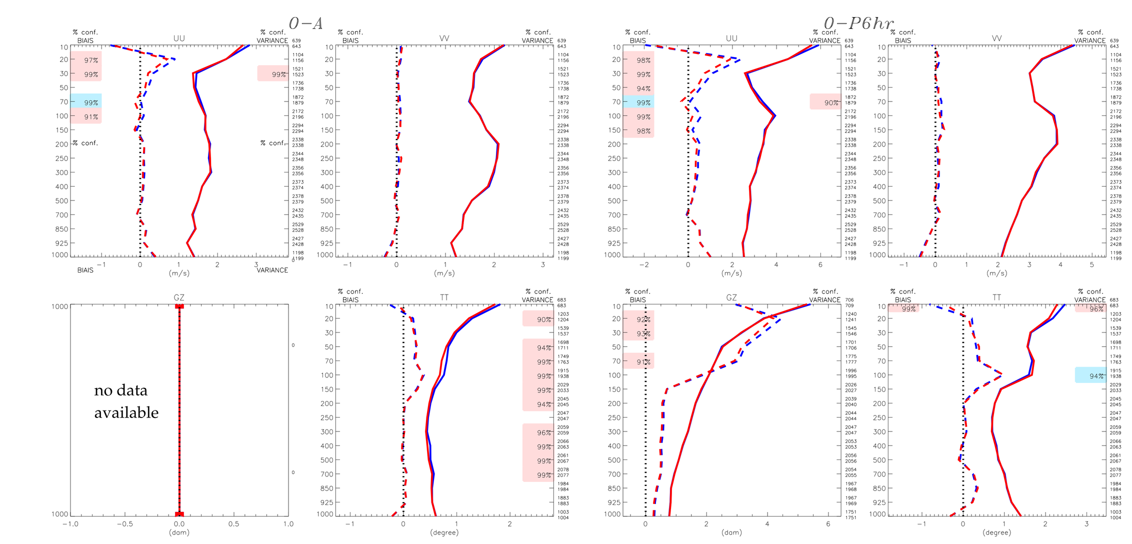

Scores against radiosondes in the tropics for a September assimilation cycle employing CBQG (red curves) are compared with the control, SB case (blue curves). With CBQG both O-A and O-P zonal velocity bias is improved in the lower stratosphere. The same holds for cycles in January. A small improvement with CBQG is also visible in the O-A temperature standard deviation and O-P geopotential height. Otherwise differences are not significant.

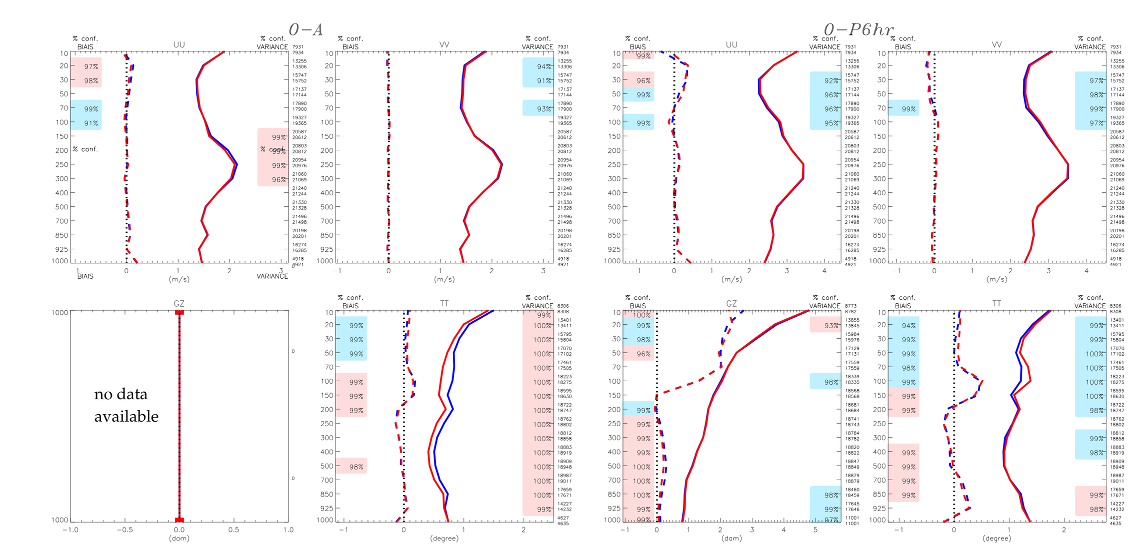

Global scores against radiosondes are shown for the cycles above. CBQG significantly improves the O-A temperature standard deviation at all radiosonde heights, however the O-P temperature standard deviation deteriorates somewhat above 200 hPa. Similar results hold for the northern and southern hemisphere individually, and likewise for January cycles.

5 Discussion

Both the Charney and QG omega constraints induce flow dependence on increments in 3D-Var, as shown by one-obs experiments. On average, the control variables are found to be more decorrelated for the Charney balance than for the statistical balance, particularly in the upper atmosphere. As implemented here, the QG omega constraint has a relatively small effect in this respect. Regarding scores against radiosondes, the new balances improve both the O-A and O-P bias for the zonal velocity in the tropics. Elsewhere results are mixed, i.e. O-A scores decrease however O-P scores increase. Unlike the statistical balance, which is time-averaged, the Charney and QG omega operators are not averaged or smoothed, and thus, tend to produce relatively noisy fields. The resulting small-scale features may themselves spawn spurious gravity waves, which would explain why, in the extratropics, the impact on O-A scores is clearly positive but tends to be negative for O-P scores. It should also be noted that only the covariances between control variables were modified. Variances and spatial correlations for each individual field were based on regression, and held fixed for all experiments. Current work is focused on the development of more consistent background statistics, as well as the introduction of diabatic forcing, similarly to [4].

Acknowledgments

The authors wish to thank M. Buehner†, L. Fillion†, C. Charette† and S. Gravel† for help with various theoretical and technical aspects of this research.

References

[1] Monge-Sanz, B. M., M. P. Chipperfield, A. J. Simmons and S. M. Uppala, 2007: Mean age of air and transport in a CTM: Comparison of different ECMWF analyses. *Geophys. Res. Lett.*, **34**, doi:10.1029/2006GL028515.

[2] Fisher, M., 2003: Background Error Covariance Modelling. *ECMWF Tech. Note.*

[3] Derber, J. and F. Bouttier, 1999: A reformulation of the background error covariance in the ECMWF global data assimilation system. *Tellus*, **51A**, 195–221.

[4] Fillion, L., M. Tanguay, E. Lapalme, B. Denis, Z. Liu, N. Ek, M. Desgagne, V. Lee and S. Pellerin, 2007: Case Dependent Implicit Normal Mode Balance Operators. *ECMWF Workshop on Flow-dependent Aspects of Data Assimilation.* Reading, England.

✉ Corresponding author's e-mail address: mateusz.reszka@ec.gc.ca